

Improving the separation efficiency of DNA biosamples in capillary electrophoresis microchips using high-voltage pulsed DC electric fields

Che-Hsin Lin · Jing-Hui Wang · Lung-Ming Fu

Received: 22 November 2007 / Accepted: 25 December 2007 / Published online: 31 January 2008
© Springer-Verlag 2008

Abstract This paper proposes a simple method for enhancing the separation efficiency of DNA biosamples in a capillary electrophoresis (CE) microchip by using high-voltage pulsed DC electric fields. A high-voltage amplifier is used to establish electric fields of up to 1 kV to carry out CE separation; electrophoresis and electroosmotic effects are then pulsedly induced. The experimental and numerical investigations commence by separating a mixed sample comprising two fluoresceins with virtually identical physical properties, namely Rhodamine B and Rhodamine 6G. It is found that the level of separation is approximately 2.1 times higher than that achieved using a conventional DC electric field of the same intensity. The performance of the proposed method is further evaluated by separating a DNA sample of *Hae*III digested Φ X-174 ladder. The experimental results indicate that the separation level of the neighboring peaks 5a and 5b in the DNA marker is approximately 1.2, which is significantly higher than the value of 0.8 obtained using a CE scheme with a conventional DC electric field. The improved separation performance of the proposed pulsed DC electric field approach is attributed to a lower Joule heating effect as a result of a lower average power input and the opportunity for

heat dissipation during the zero-voltage stage of the pulse cycle. Overall, the results demonstrate that the method proposed in this study provides a simple, low-cost technique for achieving a high separation performance in CE microchips.

Keywords Pulsed electric field · Separation efficiency · Capillary electrophoresis chip

1 Introduction

DNA separation is an essential operation in many genetic engineering processes and is commonly performed when executing biochemical and biological analyses (Bown and Meinhart 2006; Das et al. 2006; Gutsche et al. 2006; Szantai and Guttman 2006; Wang et al. 2006, 2007; Liu et al. 2007; Llopis et al. 2007; Ohashi et al. 2007; Prakash and Kaler 2007; Sun et al. 2007). However, the conventional slab-gel DNA separation method has a number of drawbacks, including a long separation time, an excessive sample consumption and a low separation efficiency. Fortunately, these limitations are largely overcome by the latest generation of micro-electro-mechanical systems (MEMS)-based DNA separation microchips. Harrison et al. (1992) first demonstrated the capillary electrophoresis (CE) separation of biosamples in a planar glass-based microchip in 1992. Compared to macro-scale separation systems, CE microchips have a number of key advantages, including a lower solvent, reagent and biosample consumption, shorter reaction times, greater portability, lower cost, improved sensitivity, lower power consumption, and the potential for parallel operation and integration with other miniaturized devices (Fu and Yang 2003; Hong and Quake 2003; Whitesides 2003). Accordingly, chip-based CE has been widely used in clinical and bio-analytical applications.

C.-H. Lin · J.-H. Wang
Department of Mechanical and Electro-Mechanical Engineering,
National Sun Yat-sen University, Kaohsiung 804, Taiwan

C.-H. Lin
Advanced Crystal Opto-electronics Research Center,
National Sun Yat-sen University, Kaohsiung 804, Taiwan

L.-M. Fu (✉)
Department of Materials Engineering, National Pingtung
University of Science and Technology,
Pingtung 912, Taiwan
e-mail: loudyfu@mail.npust.edu.tw

CE systems are generally implemented using a high-voltage DC electric field. Although the resulting driving force yields an efficient separation of the analytes within the microchannel, a strong Joule heating effect is produced during the separation procedure, which, as described below, is undesirable in CE separation applications.

The separation efficiency of a CE system is generally evaluated using the theoretical plate number, which is a function of the time required to achieve separation and the sharpness of the signal peak in the electropherogram. The theoretical plate number (N) is formulated as follows:

$$N = \frac{\mu EL}{2D}, \quad (1)$$

where μ , D , E and L are the ionic mobility ($\text{m}^2/\text{V s}$), the sample diffusion coefficient (m^2/s), the intensity of the applied electric field (V/m) and the length of the capillary channel (m), respectively. From Eq. (1), it is apparent that the theoretical plate number can be increased either by applying a higher electric field or by increasing the length of the separation channel. However, the higher electric field increases the Joule heating effect and therefore intensifies the temperature gradients in the radial and axial directions of the microchannel. Figure 1 illustrates a typical profile of the temperature gradient in the radial direction (Xuan et al. 2004). Such thermal gradients are undesirable in CE separation applications since they result in an unpredictable distribution of the buffer viscosity within the capillary. Furthermore, the diffusion coefficient (D) of the analytes increases, thereby reducing the theoretical plate number (N) [see Eq. (1)]. In addition, Joule heating effects cause the properties of the fluid, e.g., the pH of the buffer, the electric conductivity, the diffusion coefficient, the dynamic viscosity, and so forth, to become non-uniform, which affects both the applied electric potential field and the flow field (Xuan and Li 2005a) and may influence the reproducibility of the buffer (Veraart et al. 1997). It has also been reported that the Joule heating effect

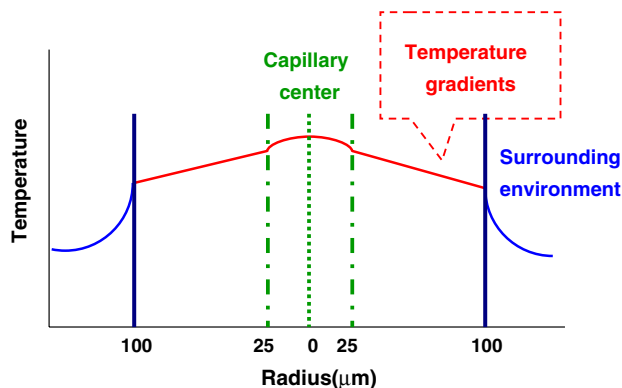


Fig. 1 Radial temperature gradient induced by Joule heating effect in capillary channel

may alter the conformations of the DNA molecules within the sample and cause the uncertain separation parameters (Guttman and Cooke 1991). Finally, Joule heating effects not only reduce the separation efficiency of the CE separation system, but also increase the buffer temperature, which in turn may prompt the thermal decomposition of unstable samples, denaturation of proteins and nucleic acids, or the production of bubbles (Rush and Cohen 1991).

From the discussions above, it is clear that Joule heating effects have a fundamental effect on the separation efficiency of CE systems. Various researchers have performed numerical and experimental investigations to clarify the influence of Joule heating on the electroosmotic flow characteristics, temperature distribution, electric field distribution, flow field structure, and sample concentration distribution within CE microchips. Li group (Xuan and Li 2004, 2005b; Xuan et al. 2004a, b) and Palonen et al. (2003, 2004) reported that the axial temperature gradient induced by Joule heating tends to broaden the signal peaks in the electropherogram and to reduce the level of separation of the analytes. Furthermore, it has been shown that the Joule heating effect increases significantly with an increasing electric field intensity, a smaller capillary size and a higher ionic strength of the buffer. Although increasing the intensity of the applied electric field increases the analyte mobility and therefore reduces the separation time, the resultant parabolic velocity profile of the fluid and the higher diffusivity of the molecules within the sample cause the sample to disperse as it travels along the capillary and therefore reduce the separation efficiency (Huang et al. 1989). Various proposals have been presented for eliminating the Joule heating effect. For example, Hjerten (1967) deliberately increased the capillary wall thickness (to achieve a 3 mm outer diameter) to enhance the heat dissipation rate by increasing the size of the convection surface. However, the performance improvement was limited. In an alternative approach, researchers integrated a microthermoelectric cooler (micro TE cooler) within the CE channel to extract the Joule heating-induced heat directly (Darabi and Ekula 2003; Rosengarten et al. 2006). However, the introduction of the micro TE cooler within the CE channel significantly complicates the chip design and fabrication processes.

Compared to the schemes presented above, the use of high-frequency pulsed DC electric fields to carry out CE separation is highly attractive since less average power is introduced into the microchannel during the separation process and hence the Joule heating effect is significantly reduced. In 1983, Schwartz et al. (1982) used a pulsed DC electric field to drive DNA samples along a zigzag path to enhance the separation efficiency under the conventional slab-gel electrophoresis system. This technique was already developed to separate DNA fragments of 10 Mbp

and upward in size (Chu 1989). However, this approach improved the separation efficiency by increasing the effective travel distance of the analytes, and hence the separation process was time-consuming and the electric control system was complex. Ghourchian and Elyasvandi (2005) used a capacitive-induced pulsed electric field to improve the separation performance of electrophoresis systems by providing an opportunity for heat dissipation between successive energy pulses. However, the proposed approach was based on a low-voltage, high-current scheme, which is applicable only for conventional slab-gel electrophoresis systems.

As shown in Fig. 2, compared to a conventional DC electric field, the use of a pulsed DC electric field reduces the power consumption for a given voltage, and hence lowers the power input into the microchannel. Furthermore, the existence of the space time during each pulse provides an opportunity for the Joule heat to dissipate before the next electric pulse is applied. As a result, a high-frequency DC pulsed electric field provides a simple and efficient means of suppressing Joule heating effects during the separation process. However, reviewing the literature, it appears that the feasibility of applying a high-voltage, low-current pulsed DC electric field to carry out DNA separation in a CE microchip has yet to be reported. Accordingly, the current study employs a standard laser-induced fluorescence detection system and a programmable high-voltage power amplifier to conduct a series of experimental investigations to evaluate the separation efficiency achieved when using high-frequency pulsed DC electric fields to carry out separation processes in a microchip-based CE system. Systematic investigations are performed to analyze the peak separation levels of a mixed sample comprising Rhodamine B and Rhodamine 6G fluorescent dyes. The electropherograms obtained under different pulsed DC power feeding conditions are compared with the results obtained using a conventional DC electric field. The optimal power feeding condition is then identified by analyzing the peak separation levels obtained under each condition at various locations of the microchannel downstream of the sample injection region. Finally, the

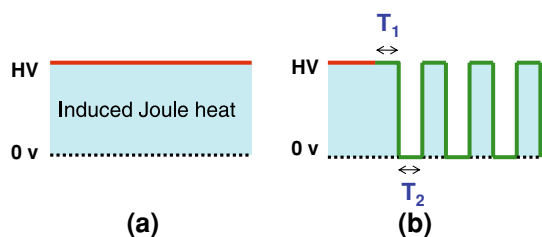


Fig. 2 Comparison of power consumption in conventional DC electric field separation process and proposed pulsed DC electric field technique

feasibility of using a high-frequency pulsed DC electric field to separate real biosamples is demonstrated using Φ X-174 DNA marker for illustration purposes. The results confirm that the proposed pulsed electric field technique provides a simple, low-cost method for reducing the Joule heating effect in CE systems.

2 Materials and methods

The CE experiments presented in this study were performed using a glass-based double-T-form microfluidic chip with a channel cross-section of $100 \times 36 \mu\text{m}$. The chip was designed with a $50\text{-}\mu\text{m}$ shift between the sample and buffer inlet channels in order to increase the size of the sample plug injected into the separation channel. The CE chip was fabricated on commercial microscope slides ($25 \times 75 \times 1 \text{ mm}$, Marienfeld, Germany) using a simple yet reliable method developed by the current authors for the rapid fabrication of microfluidic devices on planar glass substrates. The details of the fabrication procedure are presented in a previous study by the current authors and are therefore omitted here (Lin et al. 2001).

As shown in Fig. 3, the fluorescent samples were excited and observed using a standard LIF detection system comprising a fluorescence microscope (E-400, Nikon, Japan) and a mercury lamp module. Low-voltage input signals were generated using a DAQ module (USBDAQ-9100MS, Adlink Technology Inc., Taiwan) controlled by a Labview[®] program. The signals were then amplified 200X using a high-voltage power amplifier (677B-L-CE-EX, Trek Inc., USA) capable of generating an electric signal with an intensity of $\pm 2 \text{ kV}$ and a frequency varying from 0 kHz (i.e., a DC signal) to 1 kHz. The output voltage was applied to the CE microchip via a lab-built relay system. The emitted fluorescence signals were detected using a

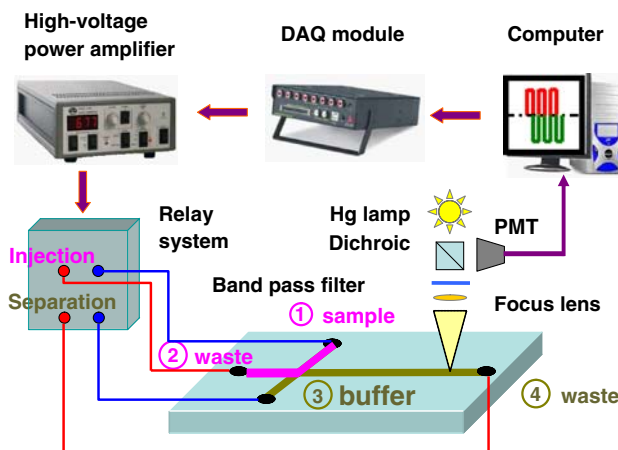


Fig. 3 Schematic illustration of experimental setup used for fluorescent sample separation investigations

PMT module (photomultiplier tube, R928, Hamamatsu Photonics, Japan) and were collected using a 16-bit DAQ (SISC, 9924, Scientific Information Service Corp., USA) card with a sampling rate of 20 Hz.

The separation performance of the proposed pulsed DC electric field approach was evaluated initially using a mixed sample comprising two fluorescent dyes, i.e., 0.5 mM Rhodamine B (479.01 g/mole, Acros Organics, USA) and 1 mM Rhodamine 6G (479.02 g/mole, Sigma-Aldrich co., USA). The viability of the proposed approach for separating real biosamples was then demonstrated using a standard DNA marker. Note that the samples were injected using the double-L injection technique to minimize sample leakage and baseline drift (Fu and Lin 2003). The physical properties of Rhodamine B and Rhodamine 6G are virtually identical and their molecular weights differ by just 0.002%. Accordingly, the mixed fluorescent sample was prepared in such a way that the concentration of Rhodamine B was five times higher than that of Rhodamine 6G to ensure that the electropherogram signals of the two dyes could be easily distinguished. The running buffer used in the CE separation tests was 10 mM $\text{Na}_2\text{B}_4\text{O}_7 \cdot 10\text{H}_2\text{O}$ (Borax, Showa chemical co., Japan) with a pH value of 9.2. The DNA separation test was performed using a standard $\Phi\text{X-174}$ RF DNA marker (HaeIII-digested, Takara Bio, Japan) with 1.5% HPMC (Sigma-Aldrich co., USA) dyeing YO-PRO-1 iodide (Molecular Probes, USA) as the sieve.

3 Numerical method

To verify the experimental separation results, a numerical model was constructed of the electrokinetic transport phenomena within the microchannel based on the spatial gradient of the electric conductivity. In constructing the model, an assumption was made that the transportation process is two-dimensional, i.e., the dependent variables do not vary in the thickness dimension of the CE chip. This assumption simplifies the numerical modeling considerably, and has been shown by Patankar and Hu (1998) to be reasonable in electroosmotic flows such as those which take place within the current double-T-form microchip. The numerical model essentially comprises a set of two-dimensional governing equations describing the distributions of the electric potential, zeta potential, ionic concentration, flow velocity, and sample concentration, respectively, throughout the computational domain.

The study investigates simple method for enhancing the separation efficiency of DNA biosamples in a capillary electrophoresis microchip by using high-voltage pulsed DC electric fields. The Joule heating effect is considered in the theoretical model. To consider electric double layer (EDL) and electrostatic field effects on fluid flow through the

microchannel, the distribution of electrical potential and net charge density between the two plates must be evaluated. The current authors developed physical models (Huang and Yang 2006) based on: (1) the Laplace equation for the applied electrostatic field ϕ , (2) the Poisson–Boltzmann equation for the EDL potential ψ , (3) the full Navier–Stokes equations modified to take account of the body force produced by the electric field and the charge density, and (4) the energy equation for temperature field. The dimensionless form of the governing equations after dropping the head symbols can be written as:

$$\frac{\partial}{\partial x_i} \left(\sigma(T) \frac{\partial \phi}{\partial x_i} \right) = 0, \quad (2)$$

$$\frac{\partial}{\partial x_i} \left(\varepsilon(T) \frac{\partial \psi}{\partial x_i} \right) = -\frac{\rho_e}{\varepsilon_0} \quad (3)$$

$$\frac{\partial u_i}{\partial x_i} = 0 \quad (4)$$

$$\rho \left(\frac{\partial u_i}{\partial t} + u_j \frac{\partial u_i}{\partial x_j} \right) = -\frac{\partial p}{\partial x_i} + \frac{\partial}{\partial x_j} \left(\mu(T) \frac{\partial u_i}{\partial x_j} \right) - \rho_e \frac{\partial(\phi + \psi)}{\partial x_i}, \quad (5)$$

$$\rho C_p \left(\frac{\partial T}{\partial t} + u_i \frac{\partial T}{\partial x_i} \right) = \frac{\partial}{\partial x_i} \left(k(T) \frac{\partial T}{\partial x_i} \right) + \sigma(T) E_i E_i + \mu(T) \frac{\partial u_i}{\partial x_j} \frac{\partial u_i}{\partial x_j}. \quad (6)$$

In these equations above, $\sigma(T)$ is the temperature-dependent electrical conductivity of liquid, $\varepsilon(T)$ is temperature-dependent permittivity, ε_0 is the permittivity of a vacuum, $\rho_e = (n^+ - n^-)ze = -2zen_0 \sinh(ze\psi/k_bT)$ is the charge density, where n^+ and n^- are the respective concentrations of the positive and negative ions, n_0 is the bulk concentration of the ions, k_b is the Boltzmann constant, T is the absolute temperature, $\mu(T)$ is the temperature-dependent liquid viscosity, C_p is the specific heat, $k(T)$ is temperature-dependent thermal conductivity, and E_i is the intensity of the externally applied electrical field. Note that the detailed derivations of the corresponding governing equations, together with their initial conditions and boundary conditions are presented by (Xuan et al. 2004a, b; Tsai et al. 2005).

4 Results and discussions

The experiments commenced by comparing the separation efficiency obtained using the proposed pulsed DC electric field technique with that achieved using a conventional DC electric field. Table 1 indicates the DC and pulsed electric field parameters considered in present investigations. The two fields are shown schematically in Fig. 2. As shown in

Table 1 DC and pulsed electric field parameters considered in present investigations

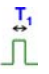

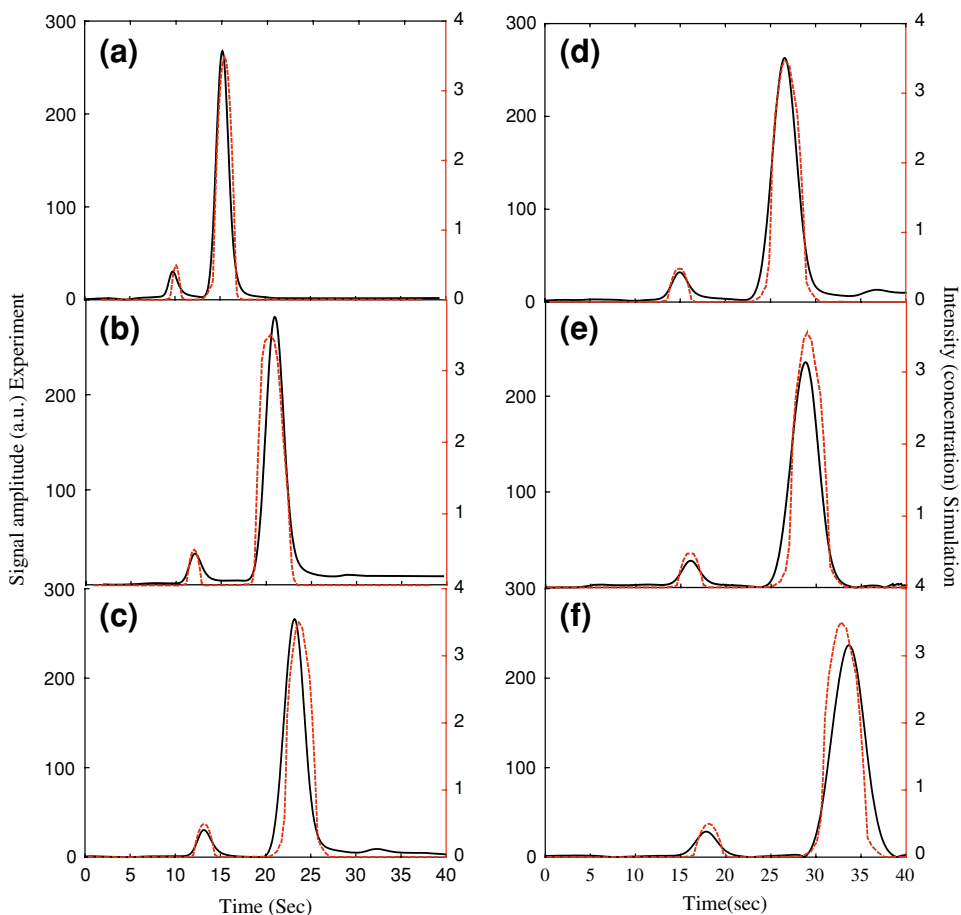
Test case	DC	1	2	3	4	5	6	7	8	9
Voltage on 		100 ms	90 ms	80 ms	70 ms	60 ms	50 ms	40 ms	30 ms	20 ms
Voltage off 	0	50 ms	50 ms	50 ms	50 ms	50 ms	50 ms	50 ms	50 ms	50 ms
On/off ratio T_2/T_1	0.00	0.50	0.56	0.63	0.71	0.83	1.00	1.25	1.67	2.50

Fig. 2b, each pulse cycle comprises two elements, namely T_1 (voltage on) and T_2 (voltage off; also known as the idle period). A short period of DC field (5 s) was applied at the beginning of the separation stage in order to drive the sample plug leaving the channel cross for the pulse DC electric fields. Figure 4 presents the experimental and numerical results obtained for the electropherogram signal amplitude at a distance 2 cm downstream from the channel cross-section when separating a mixed sample comprising 0.5 mM Rhodamine B and 1 mM Rhodamine 6G fluorescent dyes. Figure 4a corresponds to the case in which the sample is separated using a conventional DC field, while Fig. 4b–f present the results obtained using a pulsed-

electric field with voltage-on durations of $T_1 = 100, 80, 60, 50$ and 40 ms, respectively, and a constant idle period of $T_2 = 50$ ms. In every case, it can be seen that the electropherograms contain two peaks, corresponding to the two different fluorescent dyes. In other words, it is apparent that the two dyes are successfully separated using both the conventional DC electric field approach and the proposed pulsed DC electric field technique. The two fragments within the sample have an electroosmotic mobility ratio of 0.764:1 (Rhodamine B: Rhodamine 6G), and hence the peak corresponding to the Rhodamine 6G dye is detected earlier than that of the Rhodamine B dye. The peaks corresponding to Rhodamine B are taller than those of

Fig. 4 Electropherograms obtained when separating mixed sample comprising two fluorescent dyes using: **a** conventional DC electric field, and pulsed DC electric fields with **b** $T_1 = 100$ ms and $T_2 = 50$ ms, **c** $T_1 = 80$ ms and $T_2 = 50$ ms, **d** $T_1 = 60$ ms and $T_2 = 50$ ms, **e** $T_1 = 50$ ms and $T_2 = 50$ ms, and **f** $T_1 = 40$ ms and $T_2 = 50$ ms. Note detection performed 2 cm downstream from channel cross-section. Note also, DC electric field is 150 V/cm in each case



Rhodamine 6G since, as discussed previously, the concentration of the Rhodamine B dye was adjusted such that it was 5 times higher than that of Rhodamine 6G. The peak intensity of the sample concentration in the detection area is given by $C = \sum_{i=1}^N C_i/N$, where C is the average concentration intensity in the detection area, C_i is the local concentration intensity in the detection area and N is the total number of points in the detection area. In general, the results show that the non-dimensional sample fragment intensities are 3.5 (Rhodamine B) and 0.5 (Rhodamine 6G), respectively, irrespective of the power supply conditions applied. However, it can be seen that both the distance between the two peaks and the shapes of the individual peaks vary depending on the particular power supply conditions applied. Specifically, the distance between the peaks and their FWHM (full wavelength at half maxima) values increase as the idle period increases. Comparing the two DC driving modes, it is observed that the pulse mode takes slightly longer than the conventional DC mode to prompt sample diffusion and to achieve sample separation. However, the pulse mode results in a greater separation distance between the two peaks, which implies a greater level of sample separation, i.e., an improved separation performance. The results show that the separation performance is enhanced particularly at voltage-on intervals of $T_1 = 100$ and 80 ms, respectively. However, sample diffusion during the idle period may influence the separation result, even though the diffusion time is in several seconds in compared with the DC model. The peak broadening characteristic observed at longer idle periods also degrades the separation performance.

Although the separation efficiency of a CE system is generally evaluated using the theoretical plate number, a more common index for evaluating if two peak has been separated or not is the separation level (SL). The separation performance obtained using different power supply modes was analyzed using the conventional separation level (SL) index, i.e.,

$$SL = \frac{t_2 - t_1}{t_{w1} + t_{w2}}, \quad (7)$$

where t_1 and t_2 are the appearance times of the i^{th} peak (min) and the $i + 1^{\text{th}}$ peak (min), respectively, and t_{w1} and t_{w2} are the FWHMs of the i^{th} peak (min) and the $i + 1^{\text{th}}$ peak (min), respectively. In other words, the separation performance varies directly with the distance between successive peaks in the electropherograms and indirectly with the FWHM of the peaks.

Figure 5 presents the computed values of SL for the power supply modes indicated in Table 1. Note that the lines with triangular and circular symbols correspond to detection positions located 1 and 2 cm downstream from

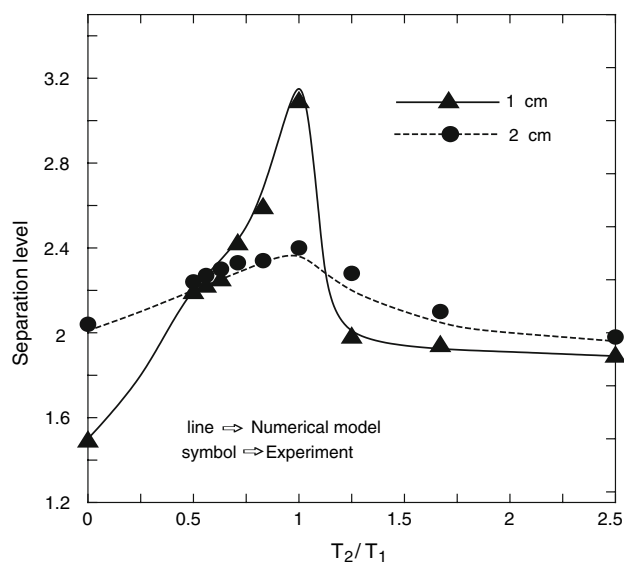


Fig. 5 Separation levels of Rhodamine B and Rhodamine 6G using conventional DC power supply mode and various pulsed electric field profiles. Note *solid lines marked with triangles and circles* correspond to detection zones located 1 and 2 cm downstream of the channel cross-section, respectively

the channel cross-section, respectively. In general, the results show that for a constant detection position, the proposed pulsed electric field driving mode consistently achieves a higher separation level than the conventional DC method. Furthermore, it is apparent that the optimal separation level is achieved when the voltage-on and idle-time durations are assigned equal values, i.e., $T_2:T_1 = 1$. From inspection, the optimal values of SL at detection distances located 1 and 2 cm downstream of the channel cross-section, respectively, are found to be 2.1 and 1.2 times higher than that obtained using the conventional DC electric field. These results confirm the effectiveness of the proposed method in enhancing the separation performance in a CE microchip system. However, it can be seen that diffusion effects dominate the separation performance at values of $T_2:T_1$ greater than 1. Overall, it is observed that for $T_2:T_1$ ratios lower than 0.5 or greater than 1.25, the best separation performance is achieved in the detection region located 2 cm downstream from the channel cross-section. Although, a longer separation channel increases the time available for sample diffusion, it also increases the theoretical plate number. Hence, these two effects compete with one another as the length of the separation channel is increased. However, it can be seen that the optimal separation level in the current CE chip is achieved in the detection region located 1 cm downstream from the channel cross-section when the $T_2:T_1$ ratio is assigned a value in the range 0.5–1.25. In other words, given an appropriate specification of the pulsed electric field parameters, the optimal CE separation performance can be obtained within

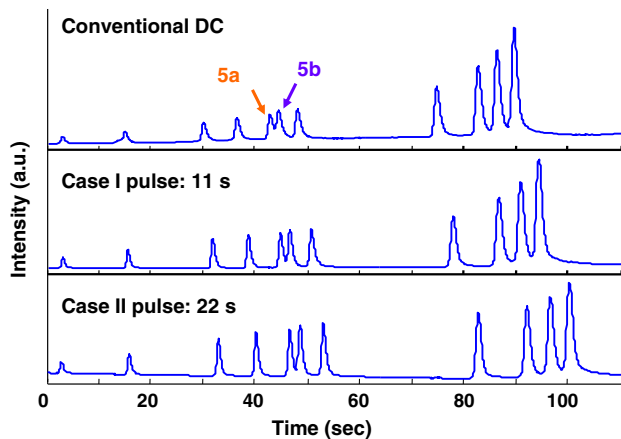


Fig. 6 Electropherograms when separating Φ X-174 DNA marker using conventional DC power supply mode and two pulsed electric field profiles. The separation levels for separating the 5a and 5b peaks in the DNA marker using the DC, Case I pulse and Case II pulse electric fields were 0.789, 1.081 and 1.216, respectively. Note that DC electric field is 300 V/cm in each case. Note also that results presented for SL indicate separation level of neighboring peaks 5a and 5b

a shorter channel length, which not only reduces the chip size, but also lowers the fabrication cost.

The separation performance of the proposed method was further evaluated using a Φ X-174 RF DNA-*Hae*III digested sample. Figure 6 presents the experimental electropherograms obtained when separating the Φ X-174 DNA marker using a conventional DC power supply mode and two pulsed power supply modes, respectively. The detection point for DNA separation located at 4 cm downstream the channel cross-section. In the conventional DC separation process, the electric field was applied for a total duration of 110 s. Meanwhile, in the Case I and Case II pulsed electric field separation processes, the pulse mode was applied for 11 s (i.e., 10% of the conventional DC separation period) and 22 s (i.e., 20% of the conventional DC separation period), respectively. Note that the magnitude of the electric field was specified as 300 V/cm in all three separation processes. It is noticed that the peaks driven using the proposed pulse DC field arrived a bit later than the sample driven using the conventional DC electric field. The delay times for the 11th peak of the Φ X-174 DNA marker for Case II and Case III were around 6 and 11 s, respectively. The results indicate that the conventional DC electric field method achieves a separation level of 0.789 between the neighboring 5a (271 bp) and 5b (281 bp) peaks in the DNA marker. By contrast, the Case I and Case II pulsed electric field methods achieve separation levels of 1.081 and 1.216, respectively. The calculated theoretical plates for peak 5b for DC field, Case I and Case II electric field methods were 62,247, 77,377 and 79,199, which also confirmed that the proposed method significantly improved the separation performance. The input electric powers for

the conventional DC electric field and the Case I and Case II pulsed power supply modes are computed to be 269.14, 256.38 and 243.64 mJ, respectively. Hence, compared to the power input of the conventional DC power supply mode, the Case I and Case II pulsed power modes reduce the total amount of power consumed (and therefore the total amount of Joule heat generated) by around 4.74 and 9.47%, respectively. Importantly, all 11 peaks of the Φ X-174 DNA marker are successfully separated within 110 s without smearing in the three electropherograms. Hence, the results confirm that the high-voltage pulsed electric field does not degrade the DNA biosample. The pulsed power supply method proposed in this study provides a higher separation performance than the conventional DC electric field. The positive experimental results are thought to be the result of lower Joule heating effects and improved heat dissipation during the separation stage.

5 Conclusions

This paper has presented a low-cost, straightforward method for enhancing the separation efficiency of CE microchips by utilizing pulsed DC electric fields. The performance of the proposed driving scheme has been verified by conducting separation experiments using a mixed fluorescent dye sample and a DNA biosample, respectively. The experimental and numerical results have demonstrated the ability of the proposed method to separate a mixed sample of Rhodamine B and Rhodamine 6G; two fluoresceins with virtually identical physical properties. It has been shown that the separation level of these two fluorescent dyes is as much as 2.1 times higher than that achieved using a conventional DC electric field. The feasibility of the proposed method has been further demonstrated via the separation of a Φ X-174 RF DNA-*Hae*III digested sample. The results have shown that the separation level of the neighboring 5a and 5b peaks can be as high as 1.2, which compares to a value of 0.8 when applying a DC electric field of the same intensity for the same duration. The enhanced separation performance of the proposed pulsed electric field scheme is thought to be the result of a lower Joule heating effect and the opportunity for heat dissipation during the idle time in each pulse. Overall, the results presented in this study confirm that the use of a pulsed DC electric field provides a viable means of achieving a high separation performance in CE microchips in a simple, low-cost manner.

Acknowledgement The authors gratefully acknowledge the financial support provided to this study by the National Science Council, Taiwan, under Grant Nos NSC94-2320-B-020-001, NSC94-2320-B-110-006 and NSC95-2314-B-020-001-MY2.

References

- Bown MR, Meinhart CD (2006) AC electroosmotic flow in a DNA concentrator. *Microfluid Nanofluid* 2:513–523
- Chu G (1989) Pulsed field electrophoresis in contour-clamped homogeneous electric-fields for the resolution of DNA by size or topology. *Electrophoresis* 10:290–295
- Darabi J, Ekula K (2003) Development of a chip-integrated micro cooling device. *Microelectron J* 34:1067–1074
- Das S, Das T, Chakraborty S (2006) Modeling of coupled momentum, heat and solute transport during DNA hybridization in a microchannel in the presence of electro-osmotic effects and axial pressure gradients. *Microfluid Nanofluid* 2:37–49
- Fu LM, Lin CH (2003) Numerical analysis and experimental estimation of a low-leakage injection technique for capillary electrophoresis. *Anal Chem* 75:5790–5796
- Fu LM, Yang RJ (2003) Low-voltage driven control in electrophoresis microchips by traveling electric field. *Electrophoresis* 24:1253–1260
- Ghourchian H, Elyasvandi H (2005) Capacitively-induced pulsed-field gel electrophoresis: a novel method for DNA separation. *Med Eng Phys* 27:723–727
- Gutsche C, Salomo M, Kim YW, Netz RR, Kremer F (2006) The flow resistance of single DNA-grafted colloids as measured by optical tweezers. *Microfluid Nanofluid* 2:381–386
- Guttman A, Cooke N (1991) Capillary gel affinity electrophoresis of DNA fragments. *Anal Chem* 63:2038–2042
- Harrison DJ, Manz A, Fan ZH, Ludi H, Widmer HM (1992) Capillary electrophoresis and sample injection systems integrated on a planar glass chip. *Anal Chem* 64:1926–1932
- Hjerten S (1967) Free zone electrophoresis. *J Chromatogr Rev* 9:122–219
- Hong JW, Quake SR (2003) Integrated nanoliter systems. *Nat Biotechnol* 21:1179–1183
- Huang KD, Yang RJ (2006) Numerical modeling of the Joule heating effect on electrokinetic flow focusing. *Electrophoresis* 27:1957–1966
- Huang XH, Coleman WF, Zare RN (1989) Analysis of factors causing peak broadening in Capillary Zone Electrophoresis. *J Chromatogr* 480:95–110
- Lin CH, Lee GB, Lin YH, Chang GL (2001) A fast prototyping process for fabrication of microfluidic systems on soda-lime glass. *J Micromech Microeng* 11:726–732
- Liu Y, Cady NC, Batt CA (2007) A plastic microchip for nucleic acid purification. *Biomed Microdevices* 9:769–776
- Llopis SL, Osiri J, Soper SA (2007) Surface modification of poly (methyl methacrylate) microfluidic devices for high-resolution separations of single-stranded DNA. *Electrophoresis* 28:984–993
- Ohashi T, Kuyama H, Hanafusa N, Togawa Y (2007) A simple device using magnetic transportation for droplet-based PCR. *Biomed Microdevices* 9:695–702
- Palonen S, Porras SP, Jussila M, Riekkola ML (2003) Peak dispersion and contributions to plate height in nonaqueous capillary electrophoresis at high electric field strengths: propanol as background electrolyte solvent. *Electrophoresis* 24:1565–1576
- Palonen S, Jussila M, Porras SP, Riekkola ML (2004) Peak dispersion and contributions to plate height in nonaqueous capillary electrophoresis at high electric field strengths: Ethanol as background electrolyte solvent. *Electrophoresis* 25:344–354
- Patankar NA, Hu HH (1998) Numerical simulation of electroosmotic flow. *Anal Chem* 70:1870–1881
- Prakash R, Kaler KVIS (2007) An integrated genetic analysis microfluidic platform with valves and a PCR chip reusability method to avoid contamination. *Microfluid Nanofluid* 3:177–187
- Rosengarten G, Mutzenich S, Kalantar-zadeh K (2006) Integrated micro thermoelectric cooler for microfluidic channels. *Exp Therm Fluid Sci* 30:821–828
- Rush RS, Cohen AS, Karger BL (1991) Influence of column temperature on the electrophoretic behavior of myoglobin and alpha-lactalbumin in high-performance capillary electrophoresis. *Anal Chem* 63:1346–1350
- Schwartz DC, Saffran W, Welsh J, Haas R, Goldenberg M, Cantor CR (1982) New techniques for purifying large DNAs and studying their properties and packaging. *Cold Spring Harb Sym* 47:189–195
- Sun Y, Kwok YC, Nguyen NT (2007) Modeling and experimental characterization of peak tailing in DNA gel electrophoresis. *Microfluid Nanofluid* 3:323–332
- Szantai E, Guttman A (2006) Genotyping with microfluidic devices. *Electrophoresis* 27:4896–4903
- Veraart JR, Gooijer C, Lingeman H (1997) Thermostating in capillary electrophoresis. *Chromatographia* 44:129–134
- Wang KG, Yue SL, Wang L, Jin AZ, Gu CZ, Wang PY, Feng YC, Wang YC, Niu HB (2006) Manipulating DNA molecules in nanofluidic channels. *Microfluid Nanofluid* 2:85–88
- Wang Y, Bedekar AS, Krishnamoorthy S, Siddhaye SS, Sundaram S (2007) System-level modeling and simulation of biochemical assays in lab-on-a-chip devices. *Microfluid Nanofluid* 3:307–322
- Whitesides GM (2003) The “right” size in nanobiotechnology. *Nat Biotechnol* 21:1161–1165
- Xuan XC, Li DQ (2004) Joule heating effects on peak broadening in capillary zone electrophoresis. *J Micromech Microeng* 14:1171–1180
- Xuan XC, Li DQ (2005a) Analytical study of Joule heating effects on electrokinetic transportation in capillary electrophoresis. *J Chromatogr A* 1064:227–237
- Xuan XC, Li DQ (2005b) Band-broadening in capillary zone electrophoresis with axial temperature gradients. *Electrophoresis* 26:166–175
- Xuan XC, Sinton D, Li DQ (2004a) Thermal end effects on electroosmotic flow in a capillary. *Int J Heat Mass Tran* 47:3145–3157
- Xuan XC, Xu B, Sinton D, Li DQ (2004b) Electroosmotic flow with Joule heating effects. *Lab Chip* 4:230–236
- Tsai CH, Yang RJ, Tai CH, Fu LM (2005) Numerical simulation of electrokinetic injection techniques in capillary electrophoresis microchips. *Electrophoresis* 26:674–686